Materials Advances

ROYAL SOCIETY OF CHEMISTRY

COMMUNICATION

View Article Online
View Journal | View Issue

Cite this: *Mater. Adv.*, 2021, 2, 3552

Received 21st March 2021,
Accepted 11th May 2021

DOI: 10.1039/d1ma00243k

rsc.li/materials-advances

A nanoporous CeO_2 nanowire array by acid etching preparation: an efficient electrocatalyst for ambient N_2 reduction†

Yuyao Ji and Xingquan Liu *

It is highly attractive but still remains a key challenge to develop earth-abundant electrocatalysts for efficient NH_3 electrosynthesis *via* the N_2 reduction reaction (NRR). In this work, a nanoporous CeO_2 nanowire array on a Ti mesh (np-CeO_2/TM) was derived from MnO_2–CeO_2/TM by acid etching of MnO_2 that acts as a pore-forming agent. In 0.1 M HCl, this catalyst achieves a high faradaic efficiency of 4.7% with a NH_3 yield of 38.6 μg h^{-1} $mg^{-1}_{cat.}$ at −0.3 V *vs.* reversible hydrogen electrode, outperforming most reported Ce-based NRR electrocatalysts under ambient conditions. It also demonstrates high electrochemical stability and excellent selectivity for NH_3 generation. The acid preparation strategy is highly valuable for future design of active NRR catalysts with desired compositions in various electrocatalysis fields.

As an important industrial chemical, NH_3 has attracted much attention as a potential energy carrier and a fertilizer precursor.[1,2] With the increase of the population and the decrease of fossil fuels, the large demand for NH_3 has become an urgent social problem, which promotes the in-depth study of artificial NH_3 production technology. Due to the need for hydrogen input and energy consumption from fossil fuels, the traditional industry for producing ammonia (350–550 °C and 150–350 atm) is an energy intensive procedure: the Haber–Bosch process results in a great deal of carbon dioxide.[3] Therefore, there is a tough importunity for the development of facile and sustainable alternative strategies for NH_3 production.

As a kind of nitrogen reduction reaction (NRR) that can synthesize NH_3 at room temperature *via* using only a high efficiency electrocatalyst,[4,5] the electrocatalytic NRR plays a significant role in attracting the attention of researchers.[6–9] Recently, considerable attention has been focused on exploring non-noble-free NRR electrocatalysts.[10–23] Porous noble metals are displayed to be effectual electrocatalysts for electrochemical storage and energy conversion,[24–26] which need to be investigated for the NRR. Instead of homogeneous metal surface, the coordinatively unsaturated active sites on phosphide surface might be beneficial for the bonding of nitrogen-related intermediates, is worth discussing in the NRR. Cerium(IV) oxide (CeO_2) has benefits of desirable electronic/ionic conductivity, and the cerium ion group plays a role as an intermediate in catalytic reaction and adsorption of gas, and is exposed.[27] Both element doping[28] and interface engineering[29] are verified productively to improve the NRR ability of catalysts. Porous nanostructures have the apparent advantage of high surface-area,[30] providing good benefit to improve the electrocatalytic NRR catalysis. It is thus trusted that constructing porous Ce-based catalysts is a good strategy to enhance the NRR activity of transition metal catalysts.

Herein, we report our finding that CeO_2 nanowires are a splendid catalyst for NH_3 synthesis under ambient conditions. The key idea is to selectively generate NP-CeO_2 nanowires with different corrosion stability, using oxalic acid on MnO_2 and CeO_2. CeO_2 achieves a high FE (4.7%) and NH_3 yield (38.6 μg h^{-1} $mg^{-1}_{cat.}$) at −0.3 V *vs.* reversible hydrogen electrode (RHE), which are notably higher than those for the MnO_2–CeO_2 precursor (NH_3 yield: 14.3 μg h^{-1} $mg^{-1}_{cat.}$, and FE: 1.6%) and most reported Ce-based NRR electrocatalysts under the conditions of 0.1 M HCl.

X-ray diffraction (XRD) results for CeO_2 (scratched down from TM) are shown in Fig. 1a. CeO_2 shows six peaks at 28.5°, 33.9°, 47.8°, 56.2°, 58.5°, and 69.1° indexed to the (111), (200), (220), (311), (222), and (400) facets of CeO_2 (JCPDS No. 43-1002), proposing the effective etching of MnO_2. As it is shown in the SEM image, MnO_2–CeO_2 nanowire arrays are anchored on TM (Fig. S1, ESI†), indicating that the construction of np-CeO_2/TM maintains the nanowire array feature (Fig. 1b). The transmission electron microscopy (TEM) image of etched np-CeO_2 is shown in Fig. 1e, which expresses a truth that the high-resolution TEM (HRTEM) supports interplanar distance of 0.313 nm corresponding to the (111) plane of CeO_2 (Fig. 1c).

The Brunauer–Emmett–Teller (BET) pore-size distribution curves of np-CeO_2 (Fig. 1e) exhibit an extensive peak centering at 8.6 nm, associated excellently with the TEM data. Meanwhile, the energy-dispersive X-ray (EDX) elemental mapping images of

School of Materials and Energy, University of Electronic Science and Technology of China, Chengdu 610054, China. E-mail: lxquan@uestc.edu.cn

† Electronic supplementary information (ESI) available. See DOI: 10.1039/d1ma00243k

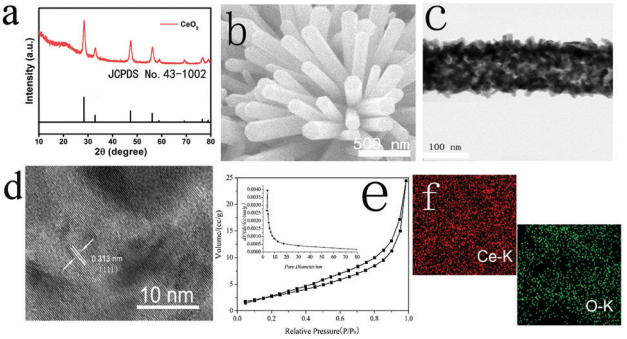

Fig. 1 (a) XRD patterns for np-CeO_2. SEM image of (b) np-CeO_2. TEM image of one single nanowire of (c) np-CeO_2. (d) HRTEM image of np-CeO_2. (e) Nitrogen adsorption/desorption isotherm plots and pore diameter of np-CeO_2. (f) EDX mapping images of CeO_2.

CeO_2 clearly show that Ce and O elements are evenly distributed on the surface. All these measurements absolutely prove the convincing formation of MnO_2–CeO_2 resulting in high surface area nanoporous CeO_2 nanowires under the condition of etching *via* acid.

X-ray photoelectron spectroscopy (XPS) was used to investigate the elemental composition and chemical valence states of porous CeO_2. As shown in Fig. 2b, high-resolution Ce 1s spectra (Fig. 2a) display binding energies of about 882.6 and 901.2 eV matching to Ce $3d_{5/2}$ and Ce $3d_{3/2}$, accordingly.[31] For O 1s, we can attribute it to three characteristic peaks. The two peaks at 530.1 and 531.7 eV correspond well to the ordered lattice oxygen ions of CeO_2, and the oxygen vacancy. For the peak at 533.3 eV, it can be defined to the absorbed hydroxyl on the surfaces of the CeO_2 from water molecules.[32,33] The difference of peak area at 531.2 eV indicated that the oxygen vacancy of CeO_2 increased significantly during hydrogen reduction after acid treatment.[34,35]

Conventional NRR is a conventional hydrogenation reduction after N_2 bubbling at the cathode surface, where H^+ could convert the electrolyte to product NH_3 by reacting with CeO_2/N_2. For our experiment, the NRR tests were conducted in a two-chamber cell separately at ambient conditions, which is partitioned by a Nafion membrane (115). For our research, the NH_3 obtained at the cathode is formed by the interaction of N_2 and H^+ by avoiding oxidation of the produced NH_3 at the anode, by avoiding passing through the spaced cell. At a moderate temperature and atmospheric pressure, the voltage was corrected by means of a reversible hydrogen electrode (RHE). The NH_3 and N_2H_4 produced by electrocatalytic reaction were determined *via* the indophenol blue

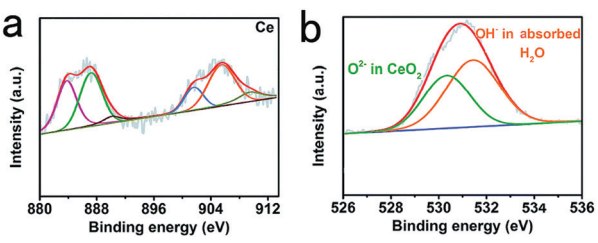

Fig. 2 XPS spectra of np-CeO_2 in the (a) Ce 3d and (b) O 1s regions.

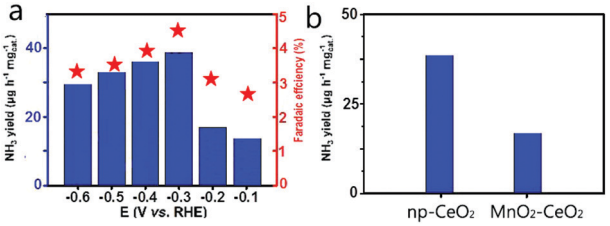

Fig. 3 (a) NH_3 yields and FEs at each given potential. (b) NH_3 yields with different catalysts at −0.3 V *vs.* RHE under ambient conditions.

method,[36] as well as by the Watt and Chrisp method.[37] The electrolyte was colored with indophenol indicator after 2 h electrocatalytic NRR reaction at constant potentials for collecting UV-Vis absorption spectra (Fig. S2 and S3, ESI†).

Np-CeO_2/GCE (0.3 mg cm^{-2}) demonstrates exceptional selectivity without N_2H_4-production (Fig. S4, ESI†). Fig. 3b exhibits average NH_3 yields, and FEs at different potentials. In the study of the effect of load on catalytic activity, it was found that when the load was 0.3 mg, the best NRR activity was shown (Fig. S5, ESI†). The optimum NRR rate is fixed at −0.3 V *vs.* RHE, causing an average yield of 38.6 μg h^{-1} mg^{-1}_{cat} NH_3, and 4.7% FE. As a catalyst with good performance, it has a great advantage over most reported NRR catalysts, including Au nanorods (6.042 μg h^{-1} mg^{-1}, 4%),[38] Cu_3P-rGO (26.38 μg h^{-1} $mg^{-1}_{cat.}$, 1.9%),[39] γ-Fe_2O_3 (0.212 μg h^{-1} $mg^{-1}_{cat.}$, 1.9%),[40] and N-doped nanocarbon (27.2 μg L^{-1} h^{-1}, 1.42%).[41] Detailed comparison is presented in Table S1 (ESI†). Fig. 3a displays that the yield increases with the increase of potential. In view of the surface competitive adsorption between N_2 and H, the catalyst performance is significantly reduced when the voltage transcends −0.3 V. For comparison, we provide hydrogen yield rates for hydrogen evolution reactions (Fig. S5, ESI†). By comparing the pH test paper of the electrolyte solution before and after electrolysis (Fig. S6, ESI†), it can be concluded that the pH hardly changed in the experiment, which shows that the whole system has not transformed through the reaction. In Fig. 3b, np-CeO_2/GCE exposits a speedier NRR rate than MnO_2–CeO_2/GCE (14.3 μg h^{-1} $mg^{-1}_{cat.}$), demonstrating that the element N plays an important role in NRR. Meanwhile, in the whole process, the weak signal value expressed by the blank GCE is completely offset. To confirm that the sensed NH_3 is produced through NRR of np-CeO_2/GCE, a series of control experiments is conducted (experimental conditions: Ar for carrier gas, −0.3 V *vs.* RHE for open-circuit potential and 20 h for electrochemical reaction). Moreover, in 0.1 M HCl, we tested the NRR performance of the nanoporous CeO_2 nanowires deposited on carbon paper, and it also shows the greatest NH_3 yield of 34.6 μg h^{-1} $mg^{-1}_{cat.}$ and a high FE of 4.6% (Fig. S7, ESI†). For comparison purposes, the NH_3 yield and FE of the MnO_2–CeO_2 are shown in Fig. S8 (ESI†), and this result also demonstrates that np-CeO_2 has better NRR performance. Meanwhile, in 0.1 M H_2SO_4, our catalyst achieves a high FE of 4.61% along with a NH_3 yield of 36.9 μg h^{-1} $mg^{-1}_{cat.}$ at −0.3 V *vs.* RHE, and it shows almost no changes when measured in 0.1 M HCl and in 0.1 M H_2SO_4 (Fig. S9, ESI†).

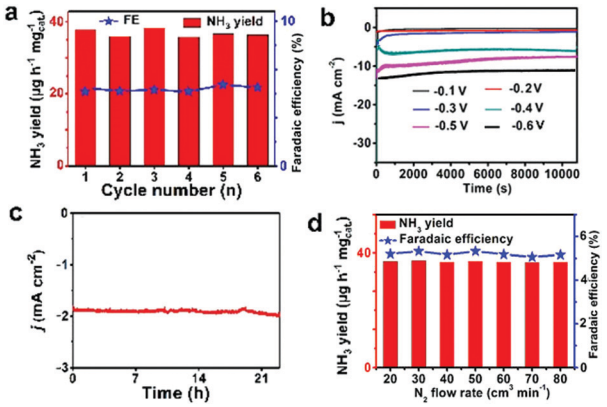

Fig. 4 (a) NH_3 yields and FEs at a potential of −0.3 V *vs.* RHE during recycling tests for 6 times. (b) Time-dependent current density curves for np-CeO_2 at different potentials. (c) Time-dependent current density curve for np-CeO_2 at −0.3 V *vs.* RHE. (d) NH_3 yields and FEs of the catalyst with different N_2 flow rates.

Stability is an additional significant parameter to estimate the catalyst behavior. Np-CeO_2/TM has insignificant changes in NH_3 yield and FE through recycling experiments for 6 times (Fig. 4a). Fig. 4b displays the long-term electrolysis at a set of potentials, which indicates good stability of np-CeO_2/TM. Moreover, a slight change occurred after the NRR reaction at −0.3 V for 24 h (Fig. 4c). The XRD (Fig. S10, ESI†) and XPS (Fig. S11, ESI†) show almost no changes before and after the long test, and they also demonstrate high electrochemical stability. The FE for np-CeO_2 demonstrates slight loss compared to the initial one after long-term testing. Based on the experimental data, it can be concluded that np-CeO_2 is exceptionally stable and durable for the NRR under ambient reaction conditions. The influence of N_2 flow rate on electrocatalytic N_2 reduction was examined concurrently. What is shown in Fig. 4d is that there is inapparent fluctuation in FEs and NH_3 yields following a series of N_2 flow-rates, suggesting that the rate of reduction is impartial to the gas–solid interface. What is more, N_2 is transported toward the cathodic catalyst surface within the N_2 of the electrolyte. In addition, since the speed of electrocatalytic reaction is independent of N_2 concentration, it can be concluded that the diffusion of N_2 is not the decisive step of the reaction.

In summary, np-CeO_2 nanowire is proven as an efficient and selective electrocatalyst for NH_3 electrosynthesis from N_2 and water in acidic media. The np-CeO_2 nanowires attain a NH_3 yield of 38.6 μg h^{-1} $mg^{-1}_{cat.}$ and an FE of 4.7% at a potential of −0.3 V. Besides, what is surprising is that np-CeO_2 possesses appealing selectivity and long-term stability for electro-hydrogenation under ambient conditions. This investigation is not only the first demonstration of applying np-CeO_2 for efficient and stable NRR electrocatalysis, but would expose a stimulating new path to the advancement of transition metal nitrides as attractive low-cost NRR catalyst materials for implementations.

Conflicts of interest

There are no conflicts to declare.

Acknowledgements

This work was supported by the National Natural Science Foundation of China (No. 21575050).

Notes and references

1 R. Schlögl, Catalytic synthesis of ammonia-a "never-ending story"?, *Angew. Chem., Int. Ed.*, 2003, **42**, 2004–2008.
2 W. Gu, Y. Guo, Q. Li, Y. Tian and K. Chu, Lithium iron oxide ($LiFeO_2$) for electroreduction of dinitrogen to ammonia, *ACS Appl. Mater. Interfaces*, 2020, **12**, 37258–37264.
3 I. Dybkjaer, In *Ammonia: catalysis and manufacture*, ed. A. Nielsen, Springer, Heidelberg, 1995, 199–308.
4 S. Li, Y. Wang, J. Liang, T. Xu, D. Ma, Q. Liu, T. Li, S. Xu, G. Chen, A. M. Asiri, Y. Luo, Q. Wu and X. Sun, TiB_2 thin film enabled efficient NH_3 electrosynthesis at ambient conditions, *Mater. Today Phys.*, 2021, **18**, 100396.
5 S. Gao, Y. Zhu, Y. Chen, M. Tian, Y. Yang, T. Jiang and Z. Wang, Self-power electroreduction of N_2 into NH_3 by 3D printed triboelectric nanogenerators, *Mater. Today*, 2019, **28**, 17–24.
6 Y. Ji, L. Li, W. Cheng, Y. Xiao, C. Li and X. Liu, A CeP nanoparticle-reduced graphene oxide hybrid: an efficient electrocatalyst for the NH_3 synthesis under ambient conditions., *Inorg. Chem. Front.*, 2021, **8**, 2103–2106.
7 T. Xu, B. Ma, J. Liang, L. Yue, Q. Liu, T. Li, H. Zhao, Y. Luo, S. Lu and X. Sun, Recent progress in metal-free electrocatalysts toward ambient N_2 reduction reaction., *Acta Phys.-Chim. Sin.*, 2021, **37**, 2009043.
8 J. Wang, L. Yu, L. Hu, G. Chen, H. Xin and X. Feng, Ambient ammonia synthesis via palladium-catalyzed electro hydrogenation of dinitrogen at low overpotential, *Nat. Commun.*, 2018, **9**, 1795.
9 K. Chu, Y. Liu, Y. Li, Y. Guo and Y. Tian, Two-dimensional (2D)/2D interface engineering of a MoS_2/C_3N_4 heterostructure for promoted electrocatalytic nitrogen fixation, *ACS Appl. Mater. Interfaces*, 2020, **12**, 7081–7090.
10 S. Chen, S. Perathoner, C. Ampelli, C. Mebrahtu, D. Su and G. Centi, Electrocatalytic synthesis of ammonia at room temperature and atmospheric pressure from water and nitrogen on a carbon-nanotube-based electrocatalyst, *Angew. Chem., Int. Ed.*, 2017, **56**, 2699–2703.
11 T. Wang, S. Li, B. He, X. Zhu, Y. Luo, Q. Liu, T. Li, S. Lu, C. Ye, A. M. Asiri and X. Sun, Commercial indium-tin oxide glass: a catalyst electrode for efficient N_2 reduction at ambient conditions, *Chin. J. Catal.*, 2021, **42**, 1024–1029.
12 C. Li, D. Ma, S. Mou, Y. Luo, B. Ma, S. Lu, G. Cui, Q. Li, Q. Liu and X. Sun, Porous $LaFeO_3$ nanofiber with oxygen vacancies as an efficient electrocatalyst for N_2 conversion to NH_3 under ambient conditions, *J. Energy Chem.*, 2020, **50**, 402–408.
13 C. Lv, Y. Qian, C. Yan, Y. Ding, Y. Liu, G. Chen and G. Yu, Defect engineering metal-free polymeric carbon nitride electrocatalyst for effective nitrogen fixation under ambient conditions, *Angew. Chem., Int. Ed.*, 2018, **57**, 10246–10250.
14 B. Ma, J. Liang, T. Li, Q. Liu, Y. Luo, S. Lu, A. M. Asiri, D. Ma and X. Sun, Iron-group electrocatalysts for ambient nitrogen

reduction reaction in aqueous media, *Nano Res.*, 2021, **14**, 555–569.

15 S. Mukherjee, D. A. Cullen, S. Karakalos, K. Liu, H. Zhang, S. Zhao, H. Xu, K. L. More, G. Wang and G. Wu, Metal-organic framework-derived nitrogen-doped highly disordered carbon for electrochemical ammonia synthesis using N_2 and H_2O in alkaline electrolytes, *Nano Energy*, 2018, **48**, 217–226.

16 T. Wang, Q. Liu, T. Li, S. Lu, G. Chen, X. Shi, A. M. Asiri, Y. Luo, D. Ma and X. Sun, Magnetron sputtered Mo_3Si thin film: an efficient electrocatalyst for N_2 reduction at ambient conditions, *J. Mater. Chem. A*, 2021, **9**, 884–888.

17 Y. Liu, M. Han, Q. Xiong, S. Zhang, C. Zhao, W. Gong, G. Wang, H. Zhang and H. Zhao, Dramatically enhanced ambient ammonia electrosynthesis performance by in-operando created Li-S interactions on MoS_2 electrocatalyst, *Adv. Energy Mater.*, 2019, **9**, 1803935.

18 Q. Li, Y. Guo, Y. Tian, W. Liu and K. Chu, Activating VS_2 basal planes for enhanced NRR electrocatalysis: the synergistic role of S-vacancies and B dopants, *J. Mater. Chem. A*, 2020, **8**, 16195–16202.

19 K. Chu, J. Wang, Y. Liu, Q. Li and Y. Guo, Mo-doped SnS_2 with enriched S-vacancies for highly efficient electrocatalytic N_2 reduction: the critical role of the Mo–Sn–Sn trimer, *J. Mater. Chem. A*, 2020, **8**, 7117–7124.

20 H. Jin, L. Li, X. Liu, C. Tang, W. Xu, S. Chen, L. Song, Y. Zheng and S. Qiao, Nitrogen vacancies on 2D layered W_2N_3: a stable and efficient active site for nitrogen reduction reaction., *Adv. Mater.*, 2019, **31**, 1902709.

21 H. Cheng, L. Ding, G. Chen, L. Zhang, J. Xue and H. Wang, Nitrogen reduction reaction: molybdenum carbide nanodots enable efficient electrocatalytic nitrogen fixation under ambient condition, *Adv. Mater.*, 2018, **30**, 1803694.

22 P. Wei, Q. Geng, A. I. Channa, X. Tong, Y. Luo, S. Lu, G. Chen, S. Gao, Z. Wang and X. Sun, Electrocatalytic N_2 reduction to NH_3 with high faradaic efficiency enabled by vanadium phosphide nanoparticle on V foil, *Nano Res.*, 2020, **13**, 2967–2972.

23 F. Wang, X. Lv, X. Zhu, J. Du, S. Lu, A. A. Alshehri, K. A. Alzahrani, B. Zheng and X. Sun, Bi nanodendrites for efficient electrocatalytic N_2 fixation to NH_3 under ambient conditions, *Chem. Commun.*, 2020, **56**, 2107–2110.

24 O. D. Velev, P. M. Tessier, A. M. Lenhoff and E. W. Kaler, Materials: a class of porous metallic nanostructures, *Nature*, 1999, **401**, 548.

25 M. Chen, Y. Zhang, L. Xing, Y. Qiu, S. Yang and W. Li, Nanoprobes: activatable photoacoustic nanoprobes for in vivo ratiometric imaging of peroxynitrite, *Adv. Mater.*, 2017, **29**, 1607015.

26 V. Malgras, H. Ataee-Esfahani, H. Wang, B. Jiang, C. Li, K. C. W. Wu, J. H. Kim and Y. Yamauchi, ChemInform abstract: nanoarchitectures for mesoporous metals, *Adv. Mater.*, 2016, **28**, 993–1010.

27 Y. Ji, J. Liu, S. Hao, Y. Xiao, L. Li and X. Liu, Full water splitting by a nanoporous CeO_2 nanowire array under alkaline conditions, *Inorg. Chem. Front.*, 2020, **7**, 2533–2537.

28 T. Wu, X. Li, X. Zhu, S. Mou, Y. Luo, X. Shi, A. M. Asiri, Y. Zhang, B. Zheng, H. Zhao and X. Sun, P-doped graphene toward enhanced electrocatalytic N_2 reduction, *Chem. Commun.*, 2020, **56**, 1831–1834.

29 W. Guo, Z. Liang, J. Zhao, B. Zhu, K. Cai, R. Zou and Q. Xu, Recent advances in graphene quantum dots: synthesis, properties, and applications, *Small Methods*, 2018, **2**, 1800204.

30 X. Zhu, S. Mou, Q. Peng, Q. Liu, Y. Luo, G. Chen, S. Gao and X. Sun, Aqueous electrocatalytic N_2 reduction for ambient NH_3 synthesis: recent advances in catalysts developing and performances boosting, *J. Mater. Chem. A*, 2020, **8**, 1545–1556.

31 K. Chu, Y. Cheng, Q. Li, Y. Liu and Y. Tian, Fe-doping induced morphological changes oxygen vacancies and Ce^{3+}–Ce^{3+} pairs in CeO_2 for promoting electrocatalytic nitrogen fixation, *J. Mater. Chem. A*, 2020, **8**, 5865–5873.

32 K. Chu, Q. Li, Y. Cheng and Y. Liu, Efficient electrocatalytic nitrogen fixation on $FeMoO_4$ nanorods, *ACS Appl. Mater. Interfaces*, 2020, **12**, 11789–11796.

33 K. Chu, Y. Liu, Y. Cheng and Q. Li, Synergistic boron-dopants and boron-induced oxygen vacancies in MnO_2 nanosheets to promote electrocatalytic nitrogen reduction, *J. Mater. Chem. A*, 2020, **8**, 5200–5208.

34 G. Zhu, J. Zhu, W. Jiang, Z. Zhang, J. Wang, Y. Zhuang and Q. Zhang, Semimetallic MoP_2: an active and stable hydrogen evolution electrocatalyst over the whole pH range, *Nanoscale*, 2016, **8**, 8500–8504.

35 Z. Geng, X. Kong, W. Chen, H. Su, Y. Liu, F. Cai, G. Wang and J. Zeng, Oxygen vacancies in ZnO nanosheets enhance CO_2 electrochemical reduction to CO, *Angew. Chem., Int. Ed.*, 2018, **57**, 6054–6059.

36 D. Zhu, L. Zhang, R. E. Ruther and R. J. Hamers, Photo-illuminated diamond as a solid-state source of solvated electrons in water for nitrogen reduction, *Nat. Mater.*, 2013, **12**, 836–841.

37 G. W. Watt and J. D. Chrisp, Photoinactivation and carbethoxylation of leucine aminopeptidase, *Anal. Chem.*, 2012, **24**, 2006–2008.

38 D. Bao, Q. Zhang, F. Meng, H. Zhong, M. Shi, Y. Zhang, J. Yan, Q. Jiang and X. Zhang, Electrochemical reduction of N_2 under ambient conditions for artificial N_2 fixation and renewable energy storage using N_2/NH_3 cycle, *Adv. Mater.*, 2017, **29**, 1604799.

39 R. Zhao, Q. Geng, L. Chang, P. Wei, Y. Luo, X. Shi, A. M. Asiri, S. Lu, Z. Wang and X. Sun, Cu_3P nanoparticles-reduced graphene oxide hybrid: an efficient electrocatalyst to realize N_2-to-NH_3 conversion under ambient conditions, *Chem. Commun.*, 2020, **56**, 9328–9331.

40 J. Kong, A. Lim, C. Yoon, J. H. Jang, H. C. Ham, J. Han, S. Nam, D. Kim, Y.-E. Sung, J. Choi and H. S. Park, Electrochemical synthesis of NH_3 at low temperature and atmospheric pressure using a γ-Fe_2O_3 catalyst, *ACS Sustainable Chem. Eng.*, 2017, **5**, 10986–10995.

41 Y. Liu, Y. Su, X. Quan, X. Fan, S. Chen, H. Yu, H. Zhao, Y. Zhang and J. Zhao, Facile ammonia synthesis from electrocatalytic N_2 reduction under ambient conditions on N-doped porous carbon, *ACS Catal.*, 2018, **8**, 1186–1191.